Efficient and Stable Mesoscopic Perovskite Solar Cells Using a Dopant-Free D-A Co-Polymer Hole-Transport Layer

Mohammad Mahdi Tavakoli[1]*, Riccardo Po[2], Gabriele Bianchi[2], Chiara Carbonera[2], Jing Kong[1]*

[1]*Department of Electrical Engineering and Computer Science, Massachusetts Institute of Technology, Cambridge, MA 02139, USA*

[2]*Decarbonization and Environmental R&D, Eni SpA, Via Fauser 4, 28100, Novara, Italy*

*Corresponding authors: mtavakol@mit.edu (M.M.T.), jingkong@mit.edu (J.K.)

Abstract

Addressing the stability issue in perovskite solar cells (PSCs) is a crucial step for commercialization purposes. Finding novel and stable hole-transfer layer (HTL) is one of the most effective strategies to solve this problem. In this work, we synthesized a new polymeric HTL, namely poly{2,7-[(5,5-bis(3',7'-dimethyloctyl)-5H-1,8-dithia-as-indacenone]-*alt*-5,5-[5',6'-bis(octyloxy)-4',7'-di-2-thienyl-2',1',3'-benzothiadiazole]} (PDTIDTBT) indicating a great hole transporting property as compared to the commonly used spiro-OMeTAD HTL. Our polymer shows good mobility with suitable band alignment with respect to the triple A-cation perovskite film, which is comparable with the state of art polymeric HTLs. Therefore, we fabricated mesoscopic PSCs by PDTIDTBT HTL and considered interface engineering technique using a thin layer of poly(methyl methacrylate) (PMMA) at the perovskite/HTL interface. Based on these modifications, we achieved a PSC with a maximum power conversion efficiency (PCE) of 19.89%, higher than the PCE of the spiro-based PSC (19.28%). Additionally, the PDTIDTBT-based PSCs shows excellent operational and ambient stability better than the spiro ones.

Keywords: Perovskite, Solar cell, Hole-transfer layer, Stability, PDTIDTBT

Introduction

Organometallic halide perovskite materials with ABX_3 crystal structure (A: methylammonium, formamidinium, Cesium; B: Pb, Sn; X: I, Br, Cl) have made a revolution in the field of optoelectronic devices.[1-7] Owing to their excellent optoelectronic properties such as high absorption and great mobility, bandgap tunability, low-cost processing and ease of fabrication, they have been the most favorable absorber layer for the fabrication of efficient perovskite solar cells (PSCs).[8-14] Over the past decade, extensive efforts on interface and compositional engineering, surface passivation and band alignment engineering have been devoted, resulted in a certified power conversion efficiency (PCE) of 25.5%.[15-18] Beside PCE, device stability plays a key role for commercialization of the PSCs. Although many researchers have focused on this issue, the PSCs still suffer from poor stability as compared to the commercialized silicon solar cells.[19-22]

To improve the device stability, some groups modified the composition of perovskite films using various additives or two-dimensional (2D) perovskites.[23-25] Others employed interface engineering or novel transporting layers.[26,27] One of the main reasons behind poor stability is the instability of HTL materials.[28,29] It is worth pointing out that the most efficient reported PSCs were made of polymeric HTLs such as 2,2′,7,7′-tetrakis[N,N-di(4-methoxyphenyl)amino]-9,9′-spirobifluorene (spiro-OMeTAD) and poly(triaryl amine) (PTAA), which are doped by some dopants.[30,31] In fact, the role of dopant in organic HTLs is to enhance the mobility and conductivity. However, most of the dopants in HTLs are not stable under light and they could be the main reason of poor stability in the PSCs. Therefore, removing dopants from the HTL is crucial for improving the device stability. Bis(trifluoromethane)sulfonimide lithium salt (Li-TFSI) is one of the most commonly used dopants in HTLs, which is not stable in ambient condition, under humidity and light and also it can add more complexity to the fabrication process.[32] Synthesis of dopant-free organic HTLs with high mobility is desirable for the fabrication of stable PSCs. In this regard, various type of polymers have been synthesized and explored in the PSCs as dopant-free HTLs over past years, resulting in decent PCEs with improved stability.[33-35] There are plenty of dopant-free polymeric HTLs reported

in the literature over the past years, resulted in devices with PCE over 20% and improved stability.[36-39] For instance, Zhang *et al.*[39] developed an efficient dopant-free cyclopenta[hi]aceanthrylene-based D-A-D type HTL (YN3), and achieved a PCE of 18.84%, which was better than that of spiro-based device (18.41%). Lee *et al.*[40] reported a new donor–acceptor type polymeric HTL (alkoxy-PTEG), which was composed of benzo[1,2-b:4,5:*b′*]dithiophene and tetraethylene glycol (TEG) with a great solubility. They achieved a planar n-i-p PSC with a PCE of 21.2% using this polymer with a better stability. More interestingly, Zhao *et al.*[41] synthesized a new HTL polymer with 1,10-phenanthroline as the conjugated core and dual functions (4,4′-(1,10-phenanthroline-3,8-diyl)bis(N,N-bis(4-methoxyphenyl)aniline)). In fact, their polymer not only works as an HTL but also passivates the surface of the perovskite film. Using their dopant-free polymer, they reported a PSC with PCE of 22.4%, which is the best reported value in the literature for PSCs with dopant-free HTLs. This efficiency is lower than the state-of-art PCE (25.5%) and more importantly the stability is still a big challenge for commercialization purposes. Beside stability and efficiency, there are other factors such as solubility of the polymer in a green solvent, synthesis complexity, E-factor and cost of processing, which need to be considered for scale-up. Most of reported polymers in the literature have focused on efficiency and slightly stability of the PSCs and therefore, more efforts are required in this regard in order to synthesize more affordable polymer for commercialization of PSCs.

In this study, we have synthesized a new D-A co-polymer, PDTIDTBT, with good mobility and charge transfer property. We employed PDTIDTBT as an HTL in mesoscopic PSCs structure and compared the photovoltaic (PV) parameters of the PDTIDTBT-based PSCs with the spiro-based devices. PDTIDTBT shows great solubility in o-xylene (green solvent), good E-factor and low synthesis complexity, which is suitable for scale-up. Time-resolved photoluminescence (TRPL) results indicated stronger quenching effect in the PSCs with PDTIDTBT. The PDTIDTBT-based PSCs showed a maximum PCE of 17.9%, which is lower than that of spiro-based PSC (18.63%). To further enhance the PCE of PDTIDTBT-based PSCs, we engineered the band alignment of PSCs

by deposition of a thin layer of PMMA at the perovskite/HTL interface. Using band alignment engineering, the PCE of PSCs with PDTIDTBT HTL increases up to 19.89% higher than its counterpart. Moreover, the PDTIDTBT-based PSC shows superior operational stability with only 8% PCE loss after 200 h under continuous illumination.

Results and discussion

The molecular structure of the PDTIDTBT co-polymer is shown in Figure 1. PDTIDTBT was obtained by Stille cross-coupling polycondensation from 5,5-bis(trimethylstannyl)-(5',6'-dioctyloxy-4',7'-di-2-thienyl-2',1',3'-benzothiadiazole) (M1) and 2,7-dibromo-(5,5-bis(3',5'-dimethyloctyl)-5H-1,8-dithia-as-indacenone) (M2). M1 was purchased from SunaTech and M2 was synthesized according to our previous work.[42] Dithiaindacenone derivatives were characterized by an economically viable and environmentally attractive synthetic process, having E-factor values of lower than 400.[43] PDTIDTBT has a relatively low synthetic complexity (~50) and exhibits a classical donor–acceptor structure, where the strength of the two components is modulated by the insertion of an oxo electron-attracting group in the donor part and 2 electron-releasing alkoxy groups in the acceptor unit, as proved by NMR data (Figure S1). A PDTIDTBT analogue has been previously used by our groups as a donor polymer in polymer solar cells.[44]

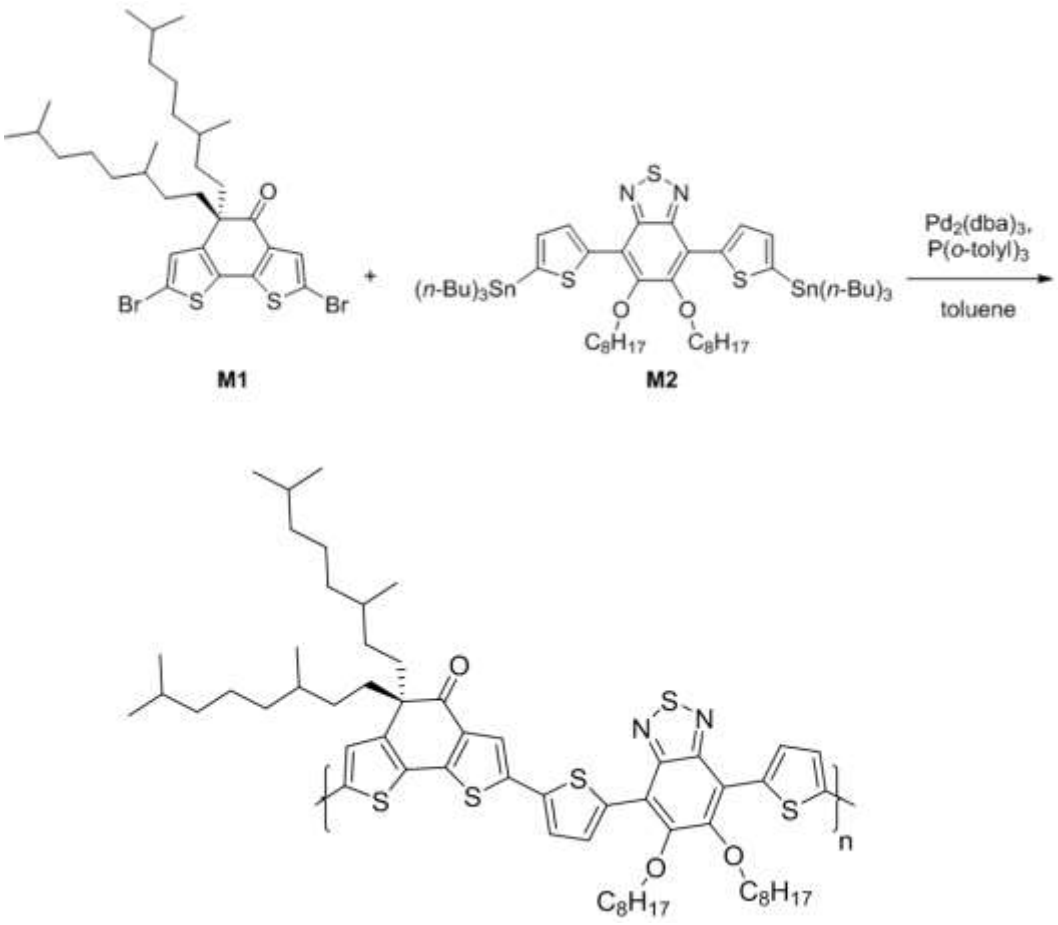

Figure 1. Molecular structure of the PDTIDTBT copolymer, resulting from the reaction of M1 and M2 molecules.

Figure S2 shows the gel permeation chromatography (GPC) measurement of the PDTIDTBT copolymer. The average molecular weight (Mw) of the PDTIDTBT was obtained to be 135497 Da. The highest occupied molecular orbital (HOMO) and lowest unoccupied molecular orbital (LUMO) levels of the PDTIDTBT were also estimated using cyclic voltammetry (CV) measurement. Figure S3 depicts the capacitance-voltage (C-V) curve of the PDTIDTBT. The results indicate HOMO and LUMO levels of -5.35 and -3.29 eV, respectively, resulting in an electrochemical bandgap of 2.06 eV. To evaluate the hole mobility of our polymer, the HTL-only device was fabricated and measured as shown in Figure S4. Using the space-charge-limited currents (SCLC) approach, the hole mobility of the PDTIDTBT was calculated to be 5.24×10^{-4} cm^2/ V.s, which is higher than that of (8.1×10^{-5} cm^2/V.s) the spiro-OMeTAD. This result confirms that the PDTIDTBT has a great

potential to be used as a dopant-free HTL in PSCs.[45] Notably, the gold electrode in the hole-only device may improve the value of mobility slightly.

Thermogravimetric analysis (TGA) of the PDTIDTBT was measured under nitrogen environment as shown in Figure 2a. From this analysis, the degradation temperature of the PDTIDTBT with 5% weight loss (T_{d95}) was estimated to be ~ 324 °C. This result indicates that the PDTIDTBT is stable at temperatures below 300 °C, suggesting its good thermal stability. Figure 2b shows the UV-visible and photoluminescence (PL) spectra of the PDTIDTBT, indicating an optical bandgap of ~1.82 eV.

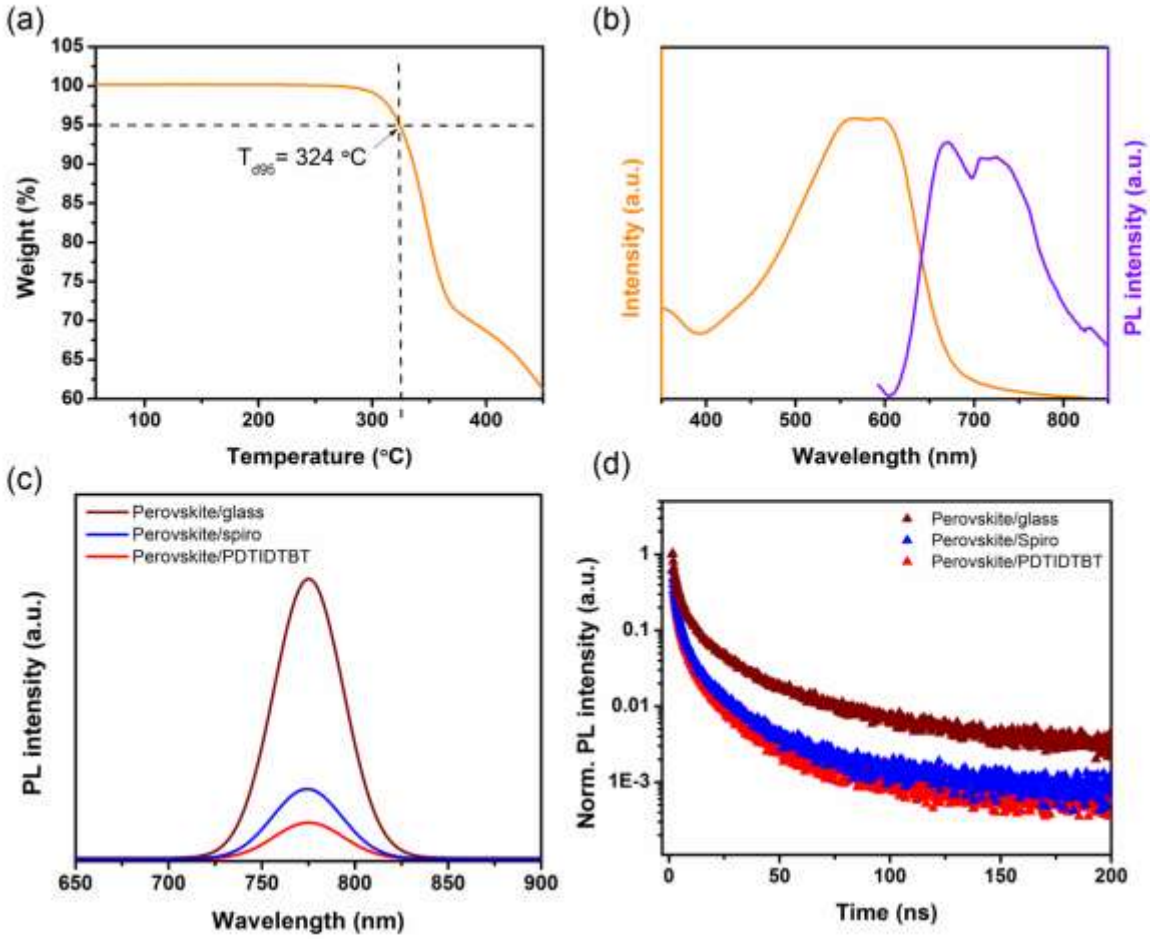

Figure 2. (a) Thermogravimetric analysis (TGA) of the PDTIDTBT copolymer measured under nitrogen at a scan rate of 10 °C/min. (b) UV-visible and photoluminescence spectra of the PDTIDTBT film. (c) Photoluminescence spectra and (d) TRPL measurement of the perovskite films on glass without and with spiro or PDTIDTBT HTLs.

From the characterization results, we concluded that it may be a good HTL alternative for the fabrication of stable perovskite solar cells. In this study, we considered triple-A cation perovskite (methylammonium (MA)/ formamidinium (FA)/cesium (Cs)) as an absorber layer. Figure S5 shows the top-view scanning electron microscopy (SEM) image and x-ray diffraction (XRD) pattern of the perovskite film, which is in good agreement with the literature. The UV-visible spectrum of the perovskite film is shown in Figure S6, indicating a band gap of 1.61 eV. Figure 2c depicts the PL spectra of the perovskite film deposited on glass without and with PDTIDTBT and spiro HTLs. As seen, the PL quenching is stronger in the perovskite/PDTIDTBT sample as compared to the spiro-based one, suggesting a better charge transfer rate than spiro. Time-resolved PL (TRPL) measurement of the corresponding films shows also the same trend as the PL results (Figure 2d). The curves were fitted by a biexponential equation. The fitting parameters are listed in Table S1. From the results, the perovskite/PDTIDTBT film shows the shortest lifetime, indicating its strong quenching effect and possibly an excellent hole transporting property.

In order to evaluate the optoelectronic properties of the PDTIDTBT, mesoscopic PSCs were fabricated with the PDTIDTBT HTL without using any dopant and the photovoltaic (PV) results were compared with the commonly used spiro HTL. Figure 3a and 3b illustrate the cross-sectional scanning electron microscopy (SEM) image and the schematic of the PDTIDTBT based PSC. As seen, the device is consisted of fluorine-doped tin oxide (FTO) as an electrode, compact layer of TiO_2 (c-TiO_2) and mesoporous TiO_2 (mp-TiO_2) and an electron transporting layer (ETL), perovskite absorber layer, PDTIDTBT HTL, and Au electrode. More details for the device fabrication can be found in the experimental section. Figure 3c shows the current density (J)-voltage (V) characteristic of the PSCs fabricated by both PDTIDTBT and spiro HTLs. Table 1 lists the PV parameters of these devices. The spiro-based device shows an open circuit voltage (V_{OC}) of 1.08 V, a short circuit current density (J_{SC}) of 22.41 mA/cm^2, a fill factor (FF) of 77%, resulting in a PCE of 18.63% under reverse scan. By changing the HTL to the PDTIDTBT, a PSC with a PCE of 17.9% is achieved (V_{OC}: 1.09 V; J_{SC}: 22.5 mA/cm^2; FF: 73%). This PV result is obtained after a thickness

optimization process. Figure S7 shows the PCE variation of the PDTIDTBT-based PSCs with different thickness of the PDTIDTBT (5-80 nm). We found that the optimum thickness of the PDTIDTBT is ~20 nm. By increase the thickness more than 20 nm, the PCE drops since the charge recombination increases at the interface of perovskite/HTL. This is mainly due to the higher series resistance of thicker HTL.[46] The inset image in Figure 3c shows the stabilized PCE of the PSCs with PDTIDTBT (17.85%) and spiro (18.58%) HTLs, confirming the results of the J-V curves. We also investigated the J_{SC} of these devices using external quantum efficiency (EQE) measurement, as shown in Figure 3d. As seen, the EQE in both cases are over 80% in the range of 350-750 nm. By integration of the solar spectrum over the entire wavelength and considering the EQE results, integrated short current densities of 21.82 mA/cm^2 and 21.69 mA/cm^2 were estimated for the PDTIDTBT and spiro based PSCs, respectively, which are in good agreement with the J-V results. The statistic PV parameter of the PSCs with both PDTIDTBT and spiro are shown in Figure S8. As seen, the average values of the V_{OC} for PDTIDTBT-based PSCs are higher than spiro-based ones. In contrast, the PSCs with PDTIDTBT HTLs shows lower FF. Overall, the average PCE value of the PSCs with PDTIDTBT HTL is 0.8% lower than the spiro-based devices. In order to further investigate the PV results, electrochemical impedance spectroscopy (EIS) was performed for both PDTIDTBT and spiro based PSCs at open circuit voltage under dark condition. Figure S9 depicts the Nyquist plots of both devices. After fitting the curves with the equivalent circuit shown in the inset image of Figure S9, the series resistance (R_S) and recombination resistance (R_{Rec}) of the corresponding devices were extracted. The R_S value of the PDTIDTBT-based PSC is 32.5 Ω, which is higher than that of (23.7 Ω) spiro based device. This can be correlated to the lower FF in the PDTIDTBT-based device. The extracted values of the R_{Rec} were 287 Ω and 196 Ω for the PDTIDTBT and spiro based PSCs, respectively. The higher value of the R_{Rec} in the PDTIDTBT device indicates lower carrier recombination[47] and as a result, this device shows higher V_{OC}.

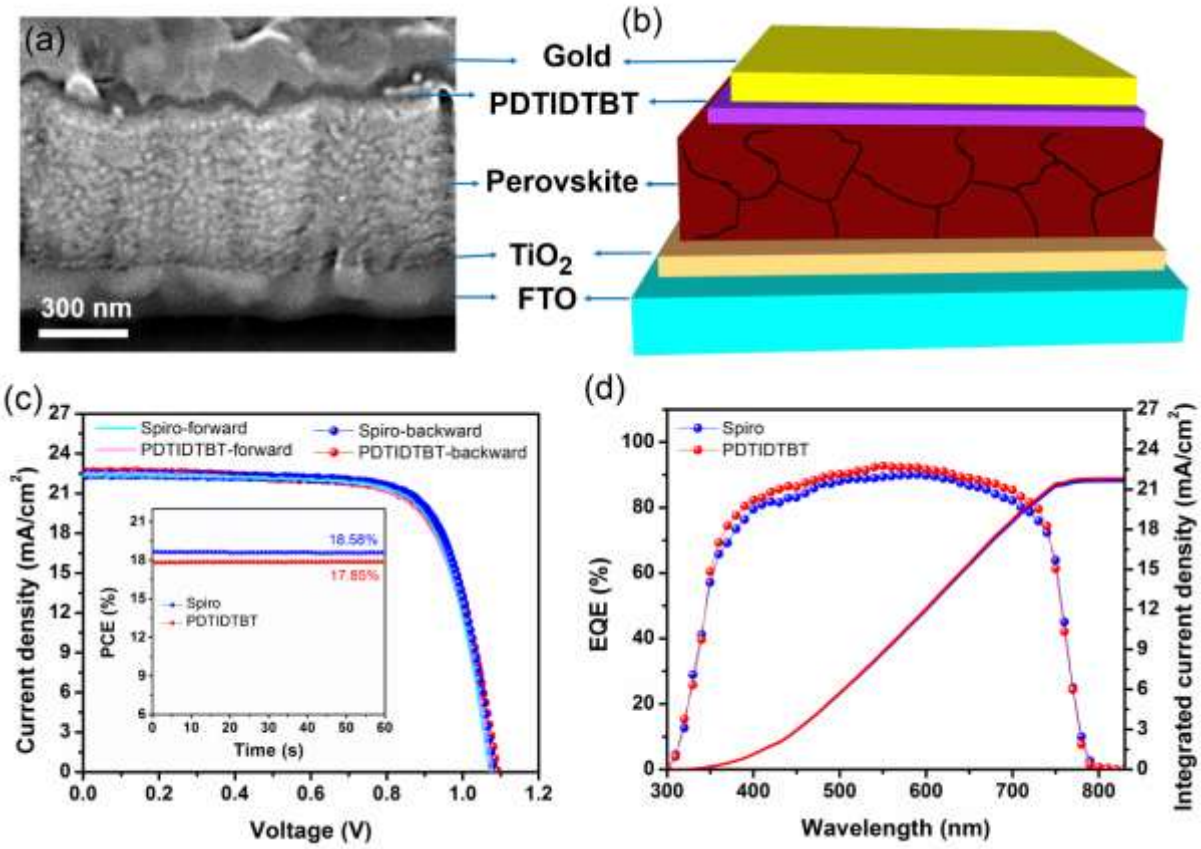

Figure 3. (a) Cross-sectional SEM image and (b) the schematic of the mesoscopic PSC fabricated by the PDTIDTBT HTL. (c) J-V curves and (d) the EQE spectra of the PSCs with the PDTIDTBT and spiro HTLs. The inset image in Figure 3c shows maximum power point tracking (MPPT) of the corresponding devices.

We also measured both devices under forward and reverse scan directions, since hysteresis effect is common phenomenon in the PSCs.[48] Figure S10 shows the statistic of the hysteresis index (HI) value for the PSCs with PDTIDTBT and spiro HTLs. Interestingly, the PDTIDTT based PSCs indicate lower HI values compared with the spiro based ones, most likely due to the better charge transfer property of the PDTIDTBT.[49]

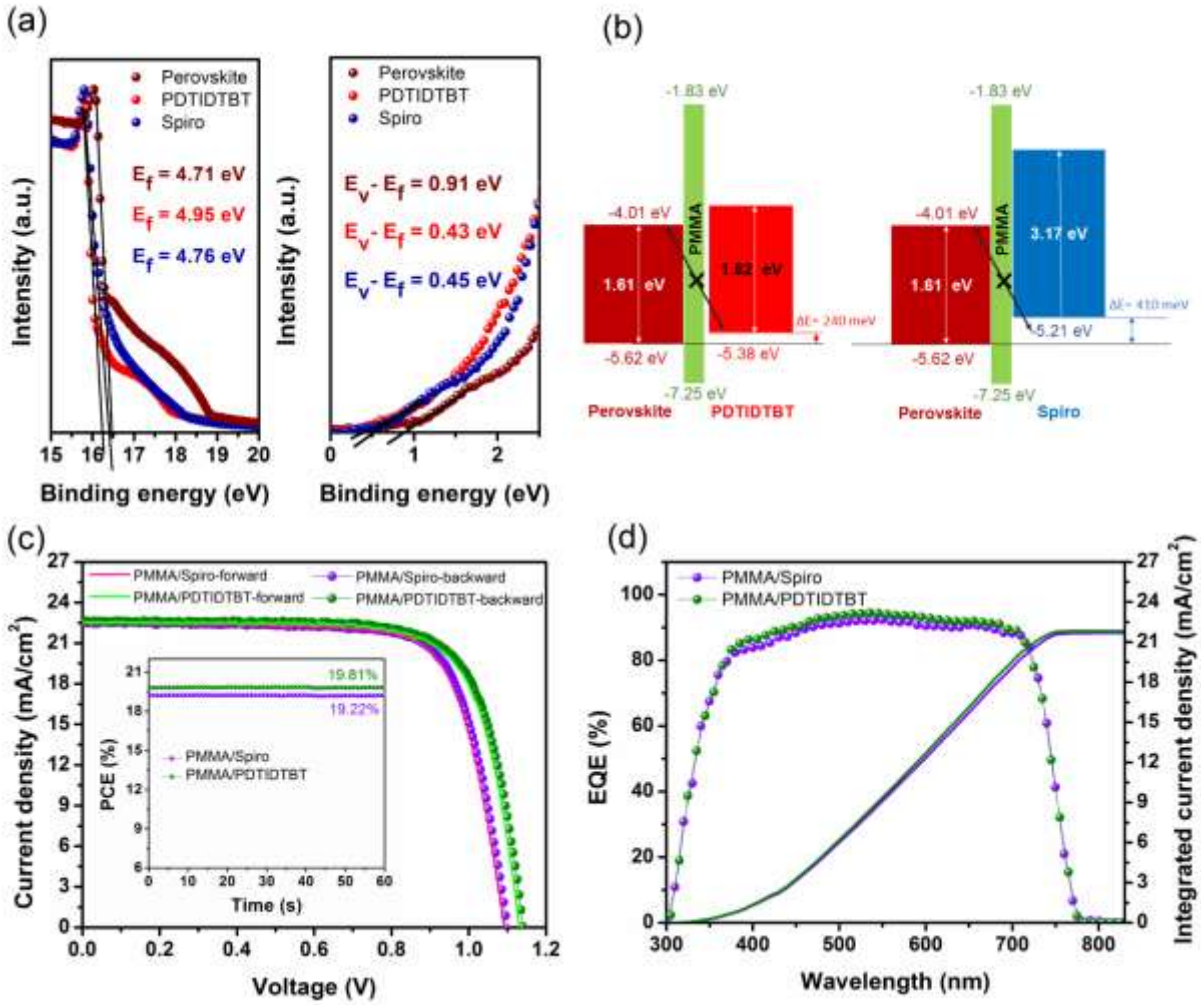

Figure 4. (a) UPS measurement of the perovskite, PDTIDTBT and spiro films. (b) Band diagram of the PSCs for both HTLs. (c) J-V curves of the PSCs with PDTIDTBT and spiro HTLs. The inset image shows the MPPT results of the corresponding devices. (d) EQE spectra of the PSCs with PDTIDTBT and spiro HTLs.

Table 1. The PV parameters of the devices with spiro and PDTIDTBT HTLs measured under reverse scan

Device	V_{oc} (V)	J_{sc} (mA/cm^2)	FF (%)	PCE (%)	MPP (%)
Spiro-backward	1.08	22.41	77	18.63	18.58
Spiro-forward	1.068	22.30	76	18.1	
PMMA/Spiro-backward	1.1	22.45	78.1	19.28	19.22
PMMA/Spiro-forward	1.09	22.43	77	18.82	

PDTIDTBT-backward	1.09	22.5	73	17.9	17.85
PDTIDTBT-forward	1.082	22.45	72.5	17.61	
PMMA/PDTIDTBT-backward	1.14	22.6	77.2	19.89	19.81
PMMA/PDTIDTBT-forward	1.132	22.51	76.7	19.54	

To further understand the reason of lower PCE in the PDTIDTBT based PSCs, the band alignment of the representative devices was plotted using ultraviolet photoelectron spectroscopy (UPS) measurement. Figure 4a shows the UPS spectra of the PDTIDTBT, spiro and perovskite films. From the UPS results, the valence band (VB) of the perovskite film, the highest occupied molecular orbital (HOMO) levels of the PDTIDTBT and spiro were estimated to be -5.62 eV, -5.38 eV and -5.21 eV, respectively. Based on UPS results and the bandgap of these films, the band diagram of the PSCs with PDTIDTBT and spiro HTLs was plotted (Figure 4b).[50,51] Our results indicate that the band offset between the perovskite and PDTIDTBT is 240 meV, which is smaller than the gap (410 meV) between the perovskite and spiro layers. This can facilitate the hole transfer from the perovskite film to the PDTIDTBT HTL more efficiently than the spiro case. As reported in the literature,[50,51] by reducing the energy gap between HTL and perovskite film, there is a great potential to reduce the interface recombination and improve the V_{OC} of the device. Ideally, the optimum band offset between the perovskite and HTL films are calculated to be in the range of 0.0-0.3 eV.[50,51] This can explain the higher V_{OC} in our PDTIDTBT based PSCs. Beside the band offset, the bandgap of the HTL is another key parameter to reduce the interface recombination. Basically, the bandgap of the HTL is required to be large enough to block the electrons efficiently. In case of the PDTIDTBT device, band gap is lower than the spiro case. This can affect on the V_{OC} and FF of the device. Additionally, the electrical properties (such as conductivity and mobility) of the PDTIDTBT is worse than the doped spiro HTL. This can be the lower FF and J_{SC} in the PDTIDTBT-based PSCs. It is worth pointing out that the charge transfer properties and also the adhesion between perovskite and HTL layers could be other effective parameters in this regard.

Consequently, to further improve the PCE of the PDTIDTBT based PSCs, we have deposited a thin layer of PMMA at the perovskite/PDTIDTBT interface. Since PMMA is an isolating layer, it can effectively reduce the recombination of the electrons from perovskite film with the holes located at the HOMO level of the PDTIDTBT.[52-54] Figure 4b shows the band diagram of the device with the PMMA layer. We also fabricated the PSCs with and without PMMA interface layer. J-V curves of the PSCs with PMMA/PDTIDTBT and PMMA/spiro are shown in Figure 4c. As seen in Table 1, the PCE of the PMMA/PDTIDTBT device is increased to 19.89%, mainly due to the enhancement of both V_{OC} and FF. Interestingly, this device shows higher PCE than the PMMA/spiro PSC (19.22%). The inset graph in Figure 4c shows the stabilized PCE of the corresponding devices, indicating the same trend as the J-V curves. This result can highlight the role of interface engineering in the PSCs and the importance of having a large bandgap HTL in the device. Figure S8 depicts the statistic PV results of the corresponding PSCs. The average value of V_{OC} and FF for the PMMA/PDTIDTBT are significantly enhanced, while the J_{SC} remains almost invariant. The PMMA modification for the PMMA/spiro also shows slightly improvement in the PV parameters. Overall, the average PCE value of the PMMA/PDTIDTBT PSCs is 0.4% higher than the PMMA/spiro one. Figure S10 shows the PL spectra of the perovskite/PMMA/PDTIDTBT and perovskite/PMMA/spiro samples. As seen, there is a strong quenching effect in perovskite/PMMA/PDTIDTBT sample, which indicates its better charge transfer properties. This result can explain the higher V_{OC} and FF in the PMMA/PDTIDTBT-based devices. Additionally, the PMMA modification can reduce the hysteresis effect of the PSCs for both cases, as shown in Figure S11, where the average HI value of the PMMA/PDTIDTBT devices is lower than the PMMA/spiro ones. This is in good agreement with the literature as well.

The main purpose of finding new HTLs for the perovskite solar cells is improving the device stability, since the stability is still the main challenge in these devices.[55,56] Figure 5a shows the shelf-life stability test of both PSCs with PMMA/PDTIDTBT and PMMA/spiro measured over 42 days in the ambient condition (42% relative humidity (RH)). The results show that the PSCs with

PMMA/PDTIDTBT retains 93% of its initial efficiency after 42 days better than the device with PMMA/spiro (74%). Additionally, we monitored the stability of our devices under continuous illumination and nitrogen flow for 110 h, as shown in Figure 5b. The operational stability results indicate that the PSC with PMMA/PDTIDTBT maintains 91% of its initial PCE much better than that of device with PMMA/spiro (52%). The higher stability of the PMMA/PDTIDTBT is mainly originated from its dopant-free nature of the PDTIDTBT HTL. Moreover, we measured the contact angle (CA) of the water droplets located on the surface of the PDTIDTBT and spiro films (Figure 5 c, d). We found that the CAs are 73° and 41° for the PDTIDTBT and spiro films, respectively, which highlights a better water-repellent property of the PDTIDTBT as compared to the spiro film. This can improve the moisture stability of the PDTIDTBT based PSCs.

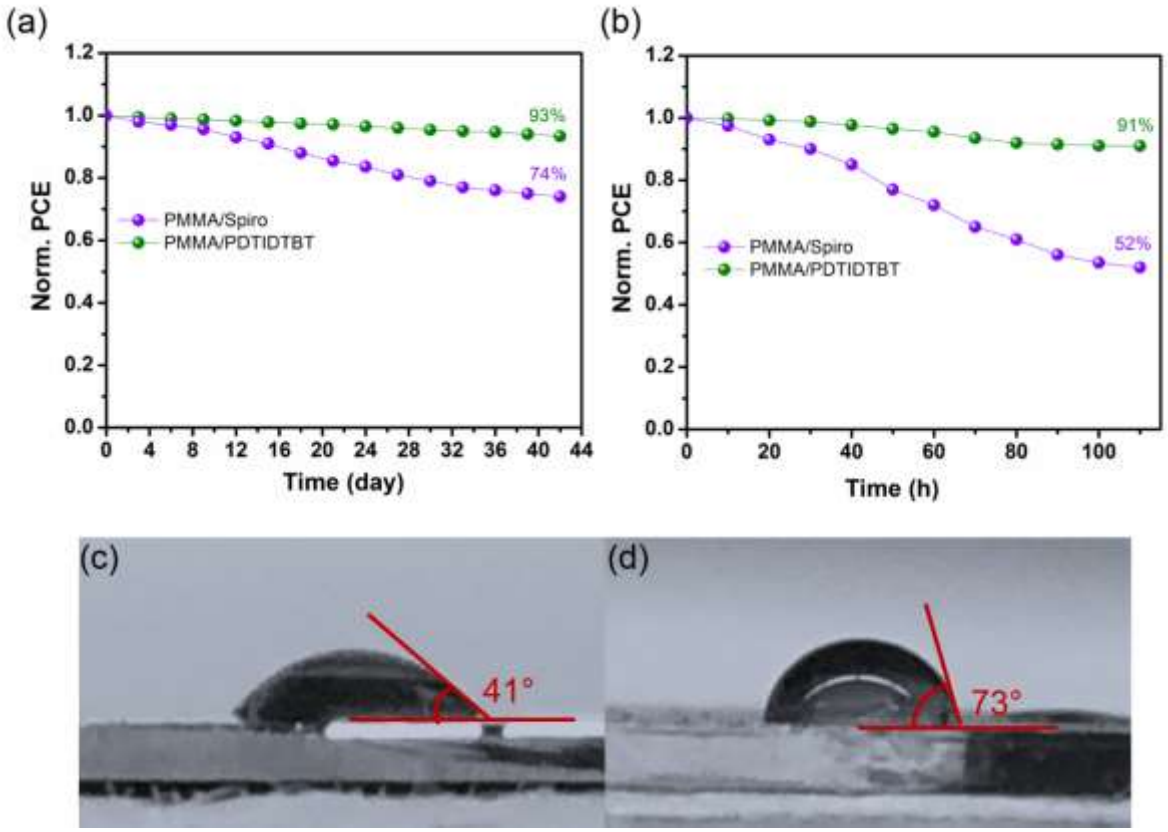

Figure 5. (a) Shelf-life stability measurement of the PSCs with PDTIDTBT and spiro HTLs measured in ambient condition over 42 days (Relative humidity (RH) was ~42%). (b) Stability measurement of the corresponding devices under continuous illumination for 110 h. Contact angle measurement of a water droplet of placed on the surface of the spiro (c) and PDTIDTBT (d) films.

Conclusions

In summary, we synthesized the PDTIDTBT, a new copolymer, with good mobility and excellent optical properties and showed its potential as an alternative HTL for the fabrication of the mesoscopic PSCs. Our characterization results indicate that the PDTIDTBT has great hole transporting property and suitable band alignment with respect to the triple-A cation perovskite. By employing interface engineering using a thin layer of PMMA, we fabricated PSCs with a dopant-free PDTIDTBT HTL and achieved an impressive PCE of 19.89%, which is better than the PCE (19.28%) of the reference device fabricated by spiro HTL. This enhancement is mainly originated from the reduction of interface recombination at the perovskite/PDTIDTBT interface using band alignment engineering. Additionally, our PDTIDTBT-based PSCs showed excellent shelf-life and operational stabilities batter than the spiro-based devices.

Experimental section

Polymerization of PDTIDTBT:

A mixture of compound M1 (SunaTech; 0.516 g, 0.80 mmol), compound M2[43] (0.908 mg, 0.80 mmol), $Pd_2(dba)_3$ (15 mg) and P(*o*-tolyl)$_3$ (19 mg) was dissolved in 50 ml of toluene. The solution was heated at 120 °C for 18h under argon. After the reaction, 2-bromobenzene (126 mg) was added and stirred at 110 °C for 4h; subsequently, 2-(tributylstannyl)thiophene (298 mg) was added and stirred at 110 °C overnight. After cooling to room temperature, the mixture was poured into 300 mL methanol. The resulting precipitate was filtered and Soxhlet extracted successively with methanol, acetone, hexane, and chloroform. The chloroform fraction was collected, concentrated to a small volume, and precipitated into 300 mL of methanol. The polymer PDTIDTBT were collected by filtration and dried under vacuum for 12 hours with a yield of 80% (0.665 g). ^{1}H NMR (400 MHz, $CDCl_3$): d = 7.5−7.8 (br, 1H), 7.3-7.4 (br, 4H), 7.0-7.2 (br, 1H), 4.1-4.4 (br, 4H), 0.6−2.3 (br, 56H). Mw = 135,497 g/mol, Mn = 67,319 g/mol, PDI = 2.01).

Device fabrication: Before any deposition the FTO glasses were etched by using zinc powder and a solution of diluted HCl, followed by cleaning in different baths using sonification: a solution of Triton X100 (1 vol% in deionized (DI) water), DI water, acetone, and isopropanol, respectively. The compact layer of TiO_2 was deposited from a solution of titanium diisopropoxide bis(acetylacetonate) dissolved in ethanol and spin-coated at 3000 rpm (1500 rpm/s ramp rate) for 30 s, followed by annealing at 500 °C for 30 min. The mesoporous TiO_2 was spin-coated at 4000 rpm for 20s (ramp rate of 2000 rpm/s) from an ethanol solution of TiO_2 paste (Dyesol 30 NR-D) diluted 6 times, followed by annealing at 500 °C for 30 min. Afterward, the TiO_2-coated substrates were cleaned by plasma for 10 min. Then, the surface of TiO_2 was treated by a solution of bis(trifluoromethane)sulfonimide lithium salt (Li-TFSI) (0.1 M in acetonitrile). The solution was spin-coated on the substrate at 4000 rpm for 20 s and annealed at 500 °C for 30 min. After this treatment, all substrates were transferred into the nitrogen-filled glovebox quickly for the next step.

The following precursors were dissolved in a mixed solvent of DMF:DMSO = 4:1 (volume ratio) at 60 °C overnight to prepare the triple-A cation (MA/FA/Cs) perovskite solution: PbI_2 (1.10 M, TCI), FAI (1.05 M, Dyesol), $PbBr_2$ (0.185 M, TCI), MABr (0.185 M, Dyesol) and 5 vol% of the CsI solution (1.5 M in DMSO). Then, the solution was spin-coated using the following steps: 1000 rpm for 10 s and 6000 rpm for 30 s. In the second step, the perovskite film was treated with anti-solvent upon applying 200 µL of chlorobenzene (CB) on the film right 10 s before the end of spinning. The perovskite films were annealed at 110 °C for 40 min. After formation of perovskite and cooling, PMMA solution (Sigma Aldrich, MW~120,000; 0.1 mg/mL in chlorobenzene) was deposited on perovskite films by spin-coating at 4000 rpm for 25 s.[57] For the HTL deposition, first, PDTIDTBT and spiro-OMeTAD were dissolved in CB with concentrations of 7 mg/mL and 80 mg/mL, respectively. For the case of spiro, 4-*tert*-butyl pyridine (4-tBP, 31.33 µL) and 18 µL of Li-TFSI solution in acetonitrile (520 mg/mL) were added into the initial solution. The prepared HTL solutions were spin-coated at 3000 rpm for PDTIDTBT and 3000 rpm for spiro on top of perovskite

films for 25 s. Finally, the device was obtained by thermal evaporation of a 100 nm-thick Au. The active area of the device was 0.1 cm^2.

Film characterization:

The cross-section and morphology of the films were characterized by a ZEISS Merlin SEM. XRD pattern was measured by Rigaku SmartLab. The PL and UV-visible spectra were evaluated by a Varian Cary 5 and a Fluorolog 322 (Horiba Jobin Ybon Ltd), respectively. TRPL measurement was performed by a picosecond pulsed diode laser (EPL-405). Excitation wavelength was 405 nm and the pulse width were 49 ps. A biexponential equation was used to fit the TRPL curves ($I(t) = a_i \exp(-t/\tau_i)$), where a_i is amplitude and τ_i is the lifetime of each component. For the UPS measurement, AXIS NOVA (Kratos Analytical Ltd, UK) was used and the UV source was the He I line (21.2 eV). TGA data were obtained by UNIX/TGA7 (PerkinElmer). The rate of heating and cooling was 10 °C/min. The cyclic voltammetry (C-V) measurement was performed using an Autolab PGSTAT 12 potentiostat. A Glassy Carbon (GC) disk in Teflon® (Amel, surface 0.071 cm^2), a platinum rod and an aqueous saturated calomel electrode (SCE, Amel) were employed as working electrode, counter electrode and as the reference electrode, respectively. For this measurement, a solution of the target polymer ($\approx 2 \cdot 10^{-4}$M) dissolved in 0.1 M tetrabutylammonium tetrafluoroborate TBATFB (Fluka, electrochemical grade, dissolved in acetonitrile) was prepared while purging argon and then analysed in the electrochemical cell with a scan rate of 200 mV s^{-1}. ^{1}H NMR spectrum was recorded by Bruker Avance 400 (400 MHz) spectrometer. The measurement was performed with 90° pulse and the relaxation delay was 1.5 s. Gel permeation chromatography (GPC) was employed to evaluate the molecular weight and measured using the following condition: Injection volume: 100 µL; Concentration: 0.1 mg/mL; flow rate: 1 mL/min and temperature was 100 °C.

To evaluate the mobility of the PDTIDTBT polymer, hole-only device was fabricated as reported in the literature.[58] For this purpose, poly(3,4-ethylenedioxythiophene):polystyrene sulfonate

(PEDOT:PSS) was first deposited on FTO by spin-coating at 2500 rpm for 40 s and annealed at 150 °C for 10 min. Then, the target HTL, i.e., PDTIDTBT (7 mg/mL in CB) was spin-coated on PEDOT:PSS-coated FTO glasses, followed by thermal evaporation of a 100-nm thick Au. Then, the device characterized by a parameter analyser to monitor the J-V curve. Using the space-charge-limited currents (SCLC) method, the mobility was estimated as reported in the literature.[58]

Device measurement:

For device measurement, a sun simulator with xenon lamp (450 W, Oriel, USA) and a digital source meter (Keithley model 2400, USA) were employed. The intensity of light was set to 1000 W/m^3 according to AM1.5G standard condition using a standard silicon solar cell (Newport). The devices were masked using a black aperture to define the active area. J-V measurement was performed at a voltage scan rate of 10 mVs^{-1}. The devices were measured under both forward and reverse scans. Notably, the hysteresis indices (HIs) was estimated by the following equation: $HI= ((PCE_{backward} - PCE_{forward})/PCE_{backward})\times100)$.[53] The EQE measurement was performed using a commercial apparatus (Arkeo-Ariadne, Cicci Research s.r.l.) with a 300 W Xenon lamp. For the shelf-life stability, the devices were kept in the dark and ambient condition (~42% RH). For the operational stability, the PSCs were kept under continuous light (1 sun) inside a nitrogen-filled glovebox. For monitoring the stability, the devices measured over time. EIS characteristic was measured close to the open circuit voltage under dark condition. The frequency was changed from 200 mHz to 100 KHz.

Acknowledgements

This work was sponsored by Eni S.p.A under the MITEI Solar Frontier Center.

References

1. N. J. Jeon, J. H. Noh, Y. C. Kim, W. S. Yang, S. Ryu, S. I. Seok, *Nat. Mater.* **2014**, *13*, 897.

2. M. M. Tavakoli, A. Waleed, L. Gu, D. Zhang, R. Tavakoli, B. Lei, W. Su, F. Fang, Z. Fan, *Nanoscale* **2017,** *9*, 5828-5834.

3. Q. Jiang, Y. Zhao, X. Zhang, X. Yang, Y. Chen, Z. Chu, Q. Ye, X. Li, Z. Yin, J. You, *Nat. Photon.* **2019**, *13*, 460–466.

4. S. Liu, Y. Guan, Y. Sheng, Y. Hu, Y. Rong, A. Mei, H. Han, *Adv. Energy Mater.* **2020**, *10*, 1902492.

5. D. Y. Son, J. W. Lee, Y. J. Choi, I. H. Jang, S. Lee, P. J. Yoo, H. Shin, N. Ahn, M. Choi, D. Kim, N. G. Park, *Nat. Energy* **2016,** *1***,** 16081.

6. A. Mahapatra, D. Prochowicz, M. M. Tavakoli, S. Trivedi, P. Kumar, P. K. Yadav, *J. Mater. Chem. A* **2020**, *8*, 27-54.

7. W. W. Liu, T. H. Wu, M. C. Liu, W. J. Niu, Y. L. Chueh, *Adv. Mater. Interfaces*, **2019**, *6*, 1801758.

8. L. Zhang, X. Zhou, C. Liu, X. Wang, B. Xu, *Small Methods*, **2020**, *4*, 2000254.

9. A. Ng, Z. Ren, Q. Shen, S. H. Cheung, H. C. Gokkaya, S. K. So, A. B. Djurišić, Y. Wan, X. Wu, C. Surya, *ACS Appl. Mater. Interfaces* **2016,** *8*, 32805.

10. M. M. Tavakoli, F. Giordano, S. M. Zakeeruddin, M. Grätzel, *Nano Lett.* **2018,** *18*, 2428-2434.

11. H. Chen, F. Ye, W. Tang, J. He, M. Yin, Y. Wang, F. Xie, E. Bi, X. Yang, M. Grätzel, L. Han, *Nature* **2017,** *550*, 92-95.

12. E. M. Sanehira, B. J. Tremolet de Villers, P. Schulz, M. O. Reese, S. Ferrere, K. Zhu, L. Y. Lin, J. J. Berry, J. M. Luther, *ACS Energy Lett.* **2016**, *1*, 38-45.

13. M. M. Tavakoli, R. Tavakoli, Z. Nourbakhsh, A. Waleed, U. S. Virk, Z. Fan, *Adv. Mater. Interfaces* **2016**, *3*, 1500790.

14. M. M. Tavakoli, R. Tavakoli, P. Yadav, J. Kong, *J. Mater. Chem. A* **2019**, *7*, 679-686.

15. National Center for Photovoltaics (NCPV) at the National Renewable Energy Laboratory (NREL), www.nrel.gov/pv/assets/images/efficiency-chart.png (accessed: March 2020).

16. G. W. Kim, H. Choi, M. Kim, J. Lee, S. Y. Son, T. Park, *Adv. Energy Mater.* **2020**, *10*, 1903403.

17. M. Kim, G. H. Kim, T. K. Lee, I. W. Choi, H. W. Choi, Y. Jo, Y. J. Yoon, J. W. Kim, J. Lee, D. Huh, H. Lee, *Joule* **2019**, *3*, 2179–2192.

18. M. M. Tavakoli, P. Yadav, D. Prochowicz, M. Sponseller, A. Osherov, V. Bulović, J. Kong, *Adv. Energy Mater.* **2019**, *9*, 1803587.

19. P. Yadav, S. H. Turren-Cruz, D. Prochowicz, M. M. Tavakoli, K. Pandey, S. M. Zakeeruddin, M. Grätzel, A. Hagfeldt, M. Saliba, *J. Phys. Chem. C*, **2018**, *122*, 15149-15154.

20. J.-C. Blancon, H. Tsai, W. Nie, C. C. Stoumpos, L. Pedesseau, C. Katan, M. Kepenekian, C. M. M. Soe, K. Appavoo, M. Y. Sfeir, S. Tretiak, P. M. Ajayan, M. G. Kanatzidis, J. Even, J. J. Crochet and A. D. Mohite, *Science*, **2017**, *355*, 1288–1292.

21. M. M. Tavakoli, M. Nasilowski, J. Zhao, M. G. Bawendi, J. Kong, *Small Methods*. **2019**, *3*, 1900449.

22. S. Zhang, Z. Liu, W. Zhang, Z. Jiang, W. Chen, R. Chen, Y. Huang, Z. Yang, Y. Zhang, L. Han, W. Chen, *Adv. Energy Mater.* **2020**, *10*, 2001610.

23. X. Zheng, B. Chen, J. Dai, Y. Fang, Y. Bai, Y. Lin, H. Wei, X. C. Zeng and J. Huang, *Nat. Energy*, **2017**, *2*, 17102.

24. Y. Cho, A. M. Soufiani, J. S. Yun, J. Kim, D. S. Lee, J. Seidel, X. Deng, M. A. Green, S. Huang, A. W. Ho-Baillie, *Adv. Energy Mater.* **2018**, *8*, 1703392.

25. M. M. Tavakoli, D. Bi, L. Pan, A. Hagfeldt, S.M. Zakeeruddin, M. Grätzel, *Adv. Energy Mater.* **2018,** *8*, 1800275.

26. Z. Yang, B. H. Babu, S. Wu, T. Liu, S. Fang, Z. Xiong, L. Han, W. Chen, *Solar Rrl*, **2020**, *4*, 1900257.

27. T. Li, Y. Pan, Z. Wang, Y. Xia, Y. Chen, W. Huang, *J. Mater. Chem. A* **2017,** *5*, 12602-12652.

28. M. M. Tavakoli, W. Tress, J. V. Milić, D. Kubicki, L. Emsley, M. Grätzel, *Energy Environ. Sci.* **2018,** *11*, 3310.

29. M. Jung, Y. C. Kim, N. J. Jeon, W. S. Yang, J. Seo, J. H. Noh, S. Il Seok, *ChemSusChem*, **2016**, *9*, 2592-2596.

30. M. M. Tavakoli, M. Saliba, P. Yadav, P. Holzhey, A. Hagfeldt, S. M. Zakeeruddin and M. Grätzel, *Adv. Energy Mater.* **2019**, *9*, 1802646.

31. G. Kakavelakis, K. Alexaki, E. Stratakis, E. Kymakis, *RSC Adv.* **2017**, *7*, 12998-13002.

32. C. Huang, W. Fu, C. Z. Li, Z. Zhang, W. Qiu, M. Shi, P. Heremans, A. K. Y. Jen, H. Chen, *JACS*, **2018**, *138*, 2528-2531.

33. M. H. Gharahcheshmeh, M. M. Tavakoli, E. F. Gleason, M. T. Robinson, J. Kong, K. K. Gleason, *Sci. Adv.* **2019**, *5*, eaay0414.

34. M. M. Tavakoli, H. T. Dastjerdi, J. Zhao, K. E. Shulenberger, C. Carbonera, R. Po, A. Cominetti, G. Bianchi, N. D. Klein, M. G. Bawendi, S. Gradecak, J. Kong, *Small*, **2019**, *15*, 1900508.

35. H. D. Pham, S. M. Jain, M. Li, Z. K. Wang, S. Manzhos, K. Feron, S. Pitchaimuthu, Z. Liu, N. Motta, J. R. Durrant, P. Sonar, *Adv. Electronic Mater.* **2020**, *6*, 1900884.

36. W. H. Lee, C. Y. Chen, C. S. Li, S. Y. Hsiao, W. L. Tsai, M. J. Huang, C. H. Cheng, C. I. Wu, H. W. Lin, *Nano Energy*, **2017**, *38*, 66-71.

37. X. Yin, Z. Song, Z. Li, W. Tang, *Energy Environ. Sci.* **2020**, *13*, 4057-4086.

38. G. You, Q. Zhuang, L. Wang, X. Lin, D. Zou, Z. Lin, H. Zhen, W. Zhuang, Q. Ling, *Adv. Energy Mater.*, **2020**, *10*, 1903146.

39. D. Zhang, P. Xu, T. Wu, Y. Ou, X. Yang, A. Sun, B. Cui, H. Sun, Y. Hua, *J. Mater. Chem. A*, **2019**, *7*, 5221-5226.

40. J. Lee, G.-W. Kim, M. Kim, S. A. Park, T. Park, *Adv. Energy Mater.*, **2020**, *10*, 1902662.

41. X. Zhao, C. Yao, K. Gu, T. Liu, Y. Xia, Y. L. Loo, *Energy Environ. Sci.* **2020**, *13*, 4334-4343.

42. G. Bianchi, R. Po, M. Sassi, L. Beverina, S. Chiaberge, S. Spera, A. Cominetti, *ACS Omega* **2017**, *2*, 4347-4355.

43. M. M. Tavakoli, R. Po, G. Bianchi, A. Cominetti, C. Carbonera, N. Camaioni, F. Tinti, J. Kong, *PNAS*, **2019**, *116*, 22037.

44. B. Xu, D. Bi, Y. Hua, P. Liu, M. Cheng, M. Grätzel, L. Kloo, A. Hagfeldt, L. Sun, *Energy Environ. Sci.* **2016**, *9*, 873-877

45. M. M. Tavakoli, R. Tavakoli, Z. Nourbakhsh, A. Waleed, U. S. Virk, Z. Fan, *Adv. Mater. Interfaces* **2016**, *3*, 1500790.

46. S. Shao, J. Liu, H. H. Fang, L. Qiu, G. H. ten Brink, J. C. Hummelen, L. J. A. Koster, M. A. Loi, *Adv. Energy Mater.* 2017, *7*, 1701305.

47. D. Y. Son, S. G. Kim, J. Y. Seo, S. H. Lee, H. Shin, D. Lee, N. G. Park, *JACS*, **2018**, *140*, 1358-1364.

48. M. M. Tavakoli, H. T. Dastjerdi, D. Prochowicz, P. Yadav, R. Tavakoli, M. Saliba, Z. Fan, *J. Mater. Chem. A*, **2019**, *7*, 14753-14760

49. M. M. Tavakoli, J. Zhao, R. Po, G. Bianchi, A. Cominetti, C. Carbonera, J. Kong, *Adv. Funct. Mater.* **2019**, *29*, 1905887.

50. T. Minemoto, M. Murata, *Sol. Energy Mater. Sol. Cells*, **2015**, *133*, 8-14.

51. X. Liu, G. Dong, L. Duan, L. Wang, Y. Qiu, *J. Mater. Chem.* **2012**, *22*, 11836-11842.

52. F. Wang, A. Shimazaki, F. Yang, K. Kanahashi, K. Matsuki, Y. Miyauchi, T. Takenobu, A. Wakamiya, Y. Murata, K. Matsuda, *J. Phys. Chem. C*, **2017**, *121*, 1562-1568.

53. S. Masi, A. Rizzo, F. Aiello, F. Balzano, G. Uccello-Barretta, A. Listorti, G. Gigli, S. Colella, *Nanoscale*, **2015**, *7*, 18956-18963.

54. F. Wang, A. Shimazaki, F. Yang, K. Kanahashi, K. Matsuki, Y. Miyauchi, T. Takenobu, A. Wakamiya, Y. Murata, K. Matsuda, *J. Phys. Chem. C*, **2017**, *121*, 1562-1568.

55. M. M. Tavakoli, L. Gu, Y. Gao, C. Reckmeier, J. He, A. L. Rogach, Y. Yao, Z. Fan, *Sci. Rep.* **2015,** *5*, 14083.

56. F. Wang, A. Shimazaki, F. Yang, K. Kanahashi, K. Matsuki, Y. Miyauchi, T. Takenobu, A. Wakamiya, Y. Murata, K. Matsuda, *J. Phys. Chem. C*, **2017**, *121*, 1562-1568.

57. W. Zhang, P. Liu, A. Sadollahkhani, Y. Li, B. Zhang, F. Zhang, M. Safdari, Y. Hao, Y. Hua, L. Kloo, *ACS Omega*, **2017**, *2*, 9231-9240.

58. M. M. Tavakoli, R. Tavakoli, D. Prochowicz, P. Yadav, M. Saliba, *Mol. Sys. Des. Eng.* **2018**, *3*, 717-722.

Supporting information

Efficient and Stable Mesoscopic Perovskite Solar Cells Using a Dopant-Free D-A Co-Polymer Hole-Transport Layer

Mohammad Mahdi Tavakoli[1]*, Riccardo Po[2], Gabriele Bianchi[2], Chiara Carbonera[2], Jing Kong[1]*

[1]*Department of Electrical Engineering and Computer Science, Massachusetts Institute of Technology, Cambridge, MA 02139, USA*

[2]*Decarbonization and Environmental R&D, Eni SpA, Via Fauser 4, 28100, Novara, Italy*

*Corresponding authors: mtavakol@mit.edu (M.M.T.), jingkong@mit.edu (J.K.)

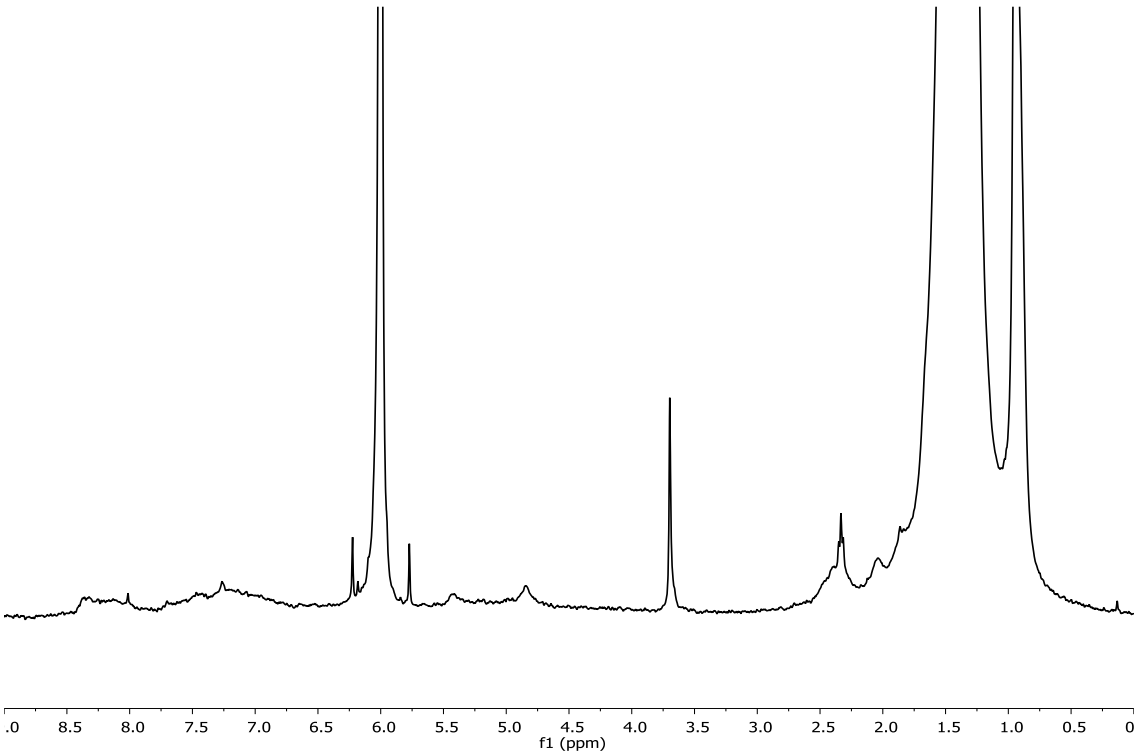

Figure S1. ^{1}H NMR spectrum of the PDTIDTBT copolymer measured at 298 K. The frequency and solvent in this measurement were 400 MHz and acetone d6, respectively.[38]

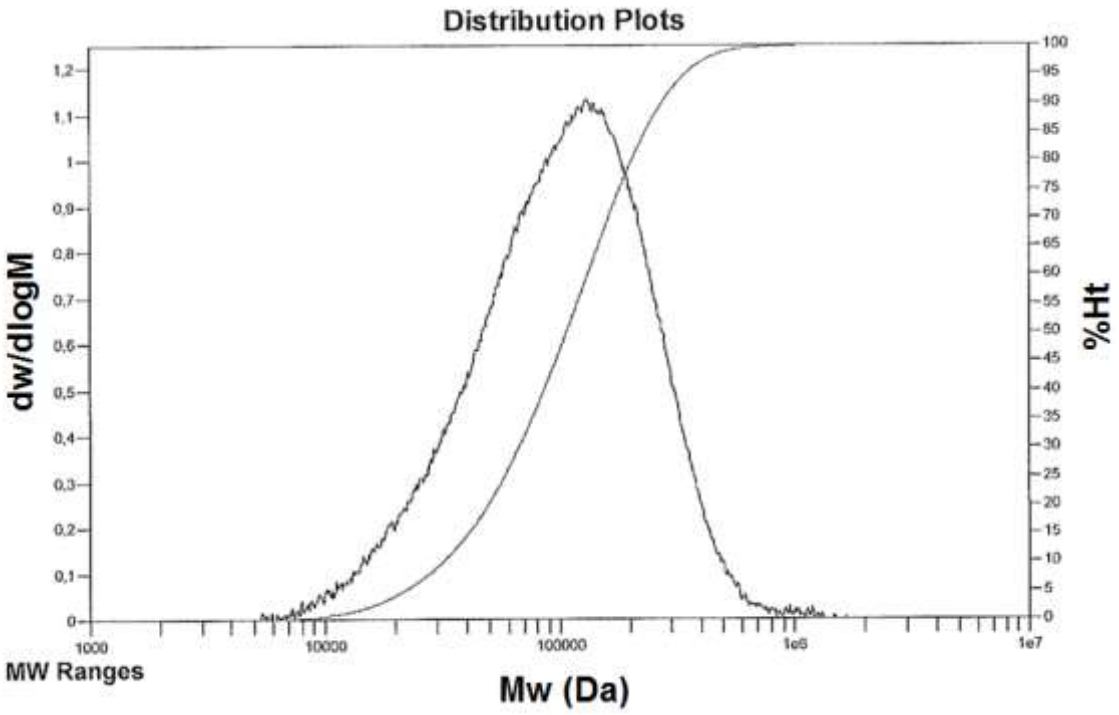

Figure S2. Molecular weight distribution of the PDTIDTBT measured by gel permeation chromatography (GPC).

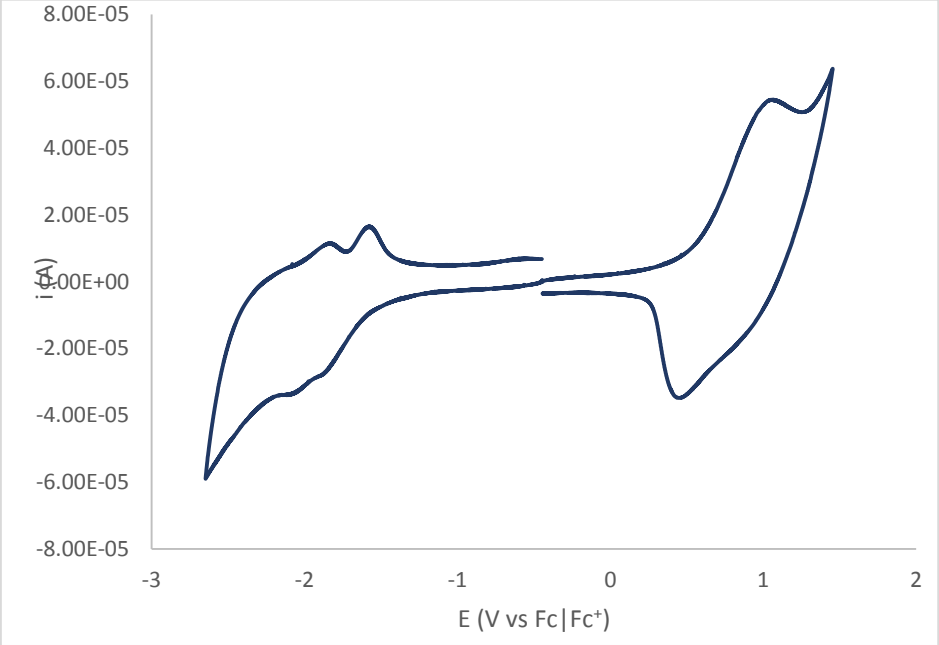

Figure S3. Capacitance-voltage measurement of the PDTIDTBT polymer dissolved in a solution of tetrabutylammonium tetrafluoroborate (TBATFB) dissolved in acetonitrile (0.1 M). The scan rate was 200 mV/s.

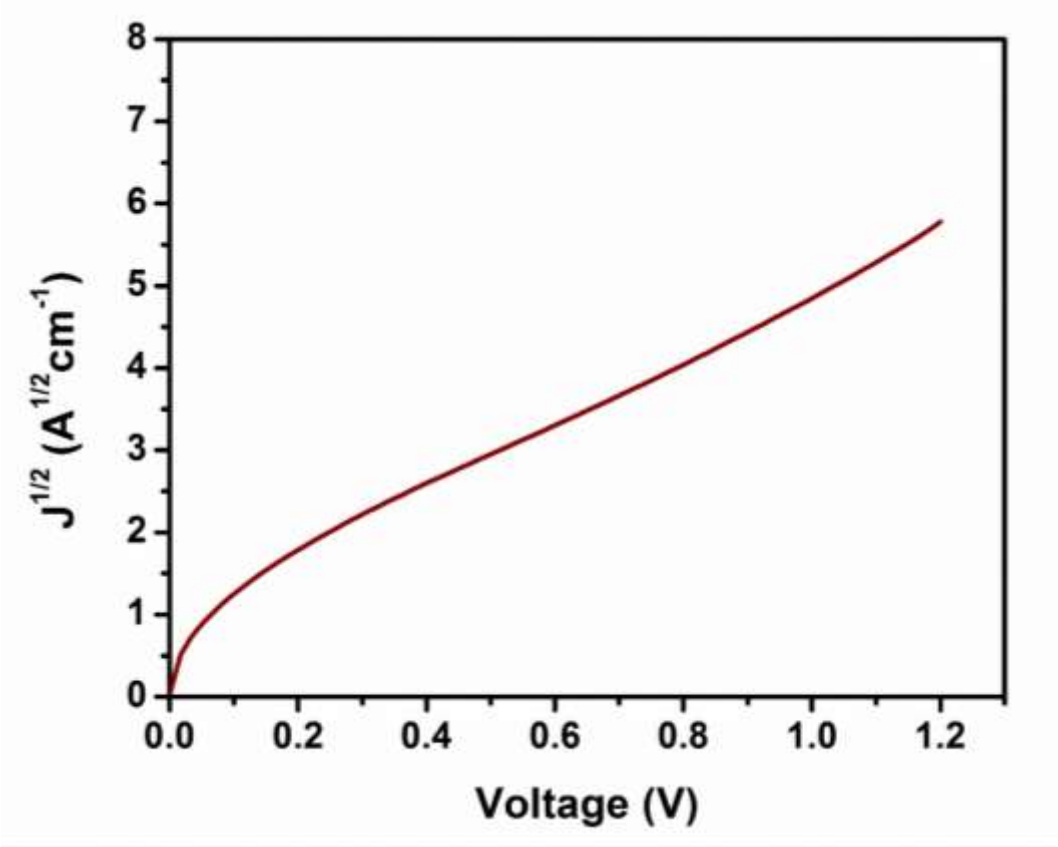

Figure S4. Current density-voltage characterization of the hole-only device fabricated by the PDTIDTBT.

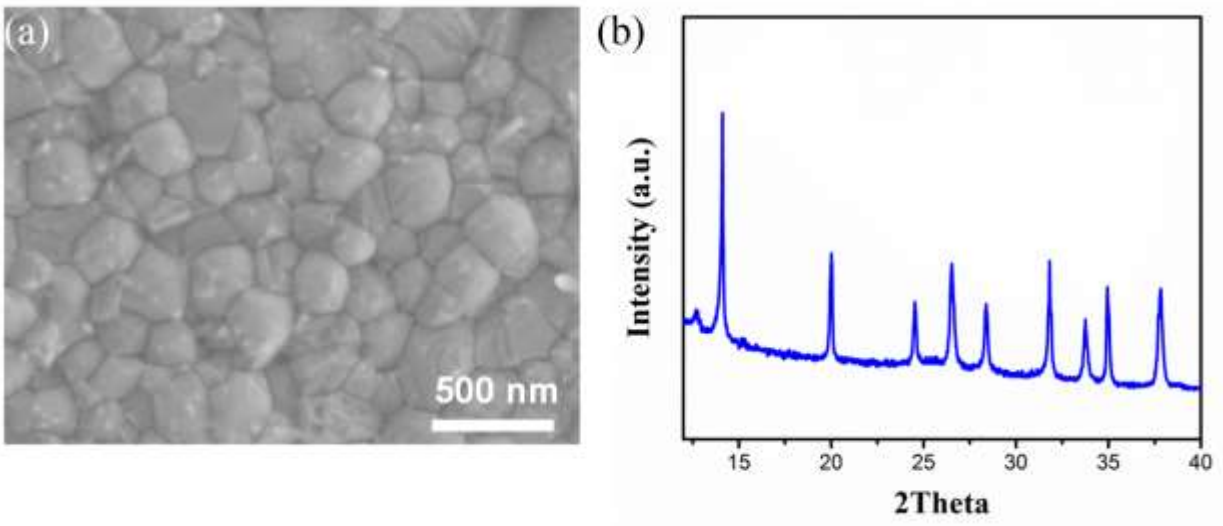

Figure S5. (a) Top-view SEM image and (b) XRD pattern of the perovskite film used in this study.

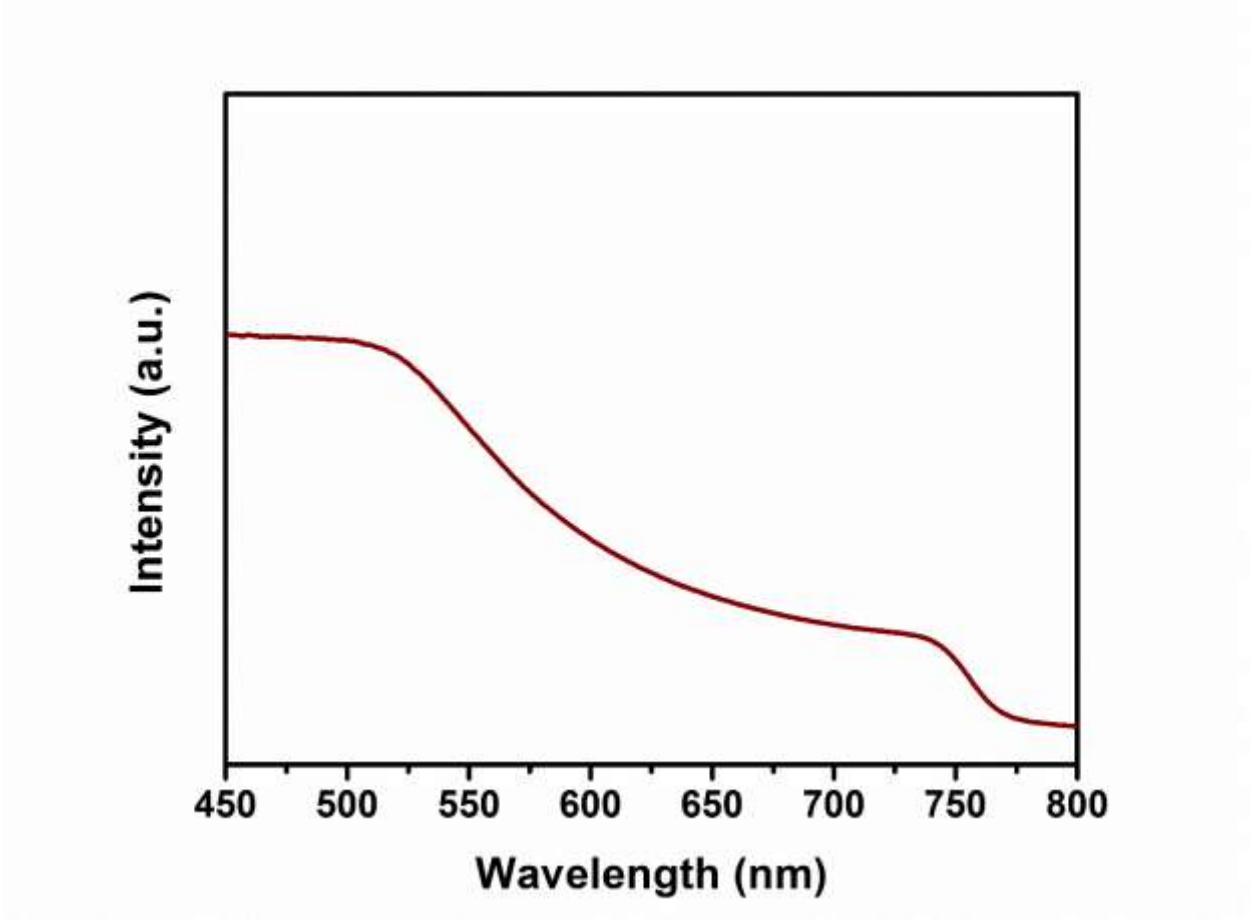

Figure S6. UV-visible spectrum of the triple-A cation perovskite film.

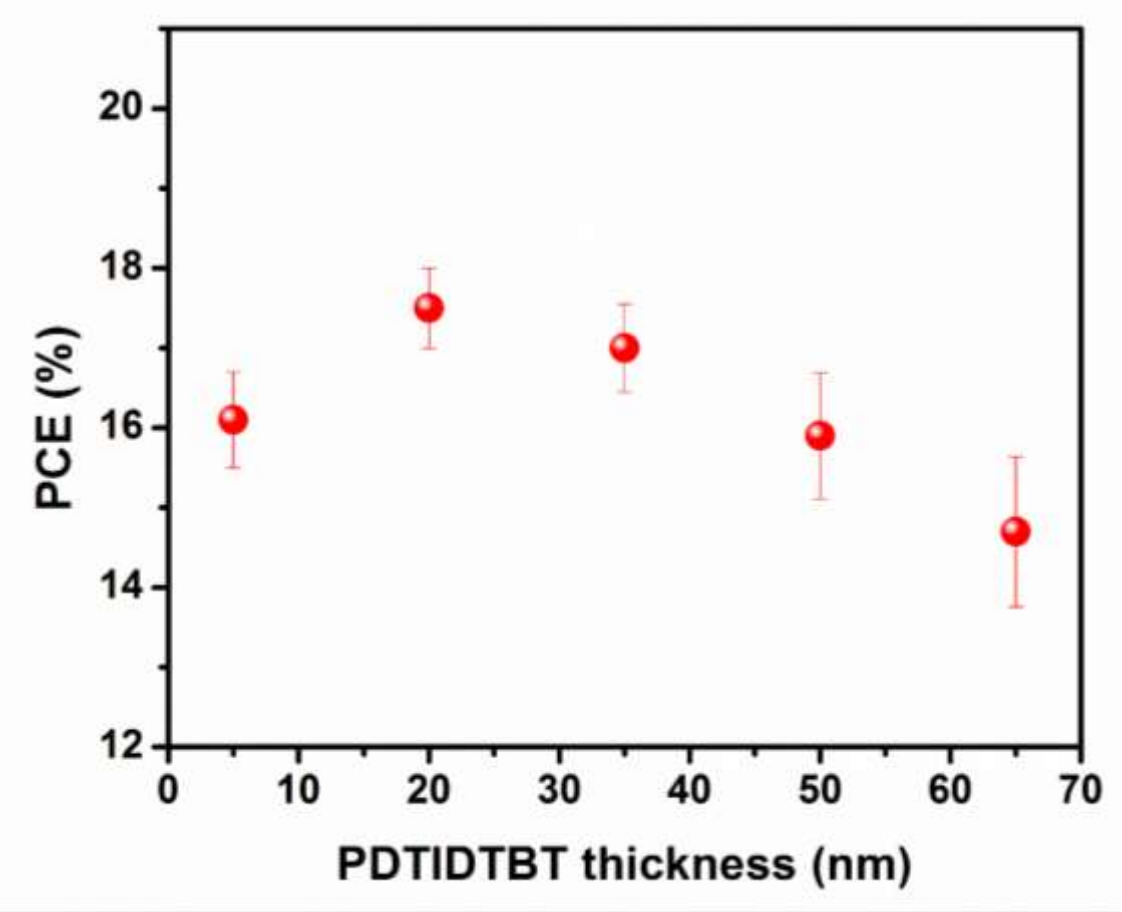

Figure S7. PCE variation of the PDTIDTBT-based PSCs with different thickness of the PDTIDTBT.

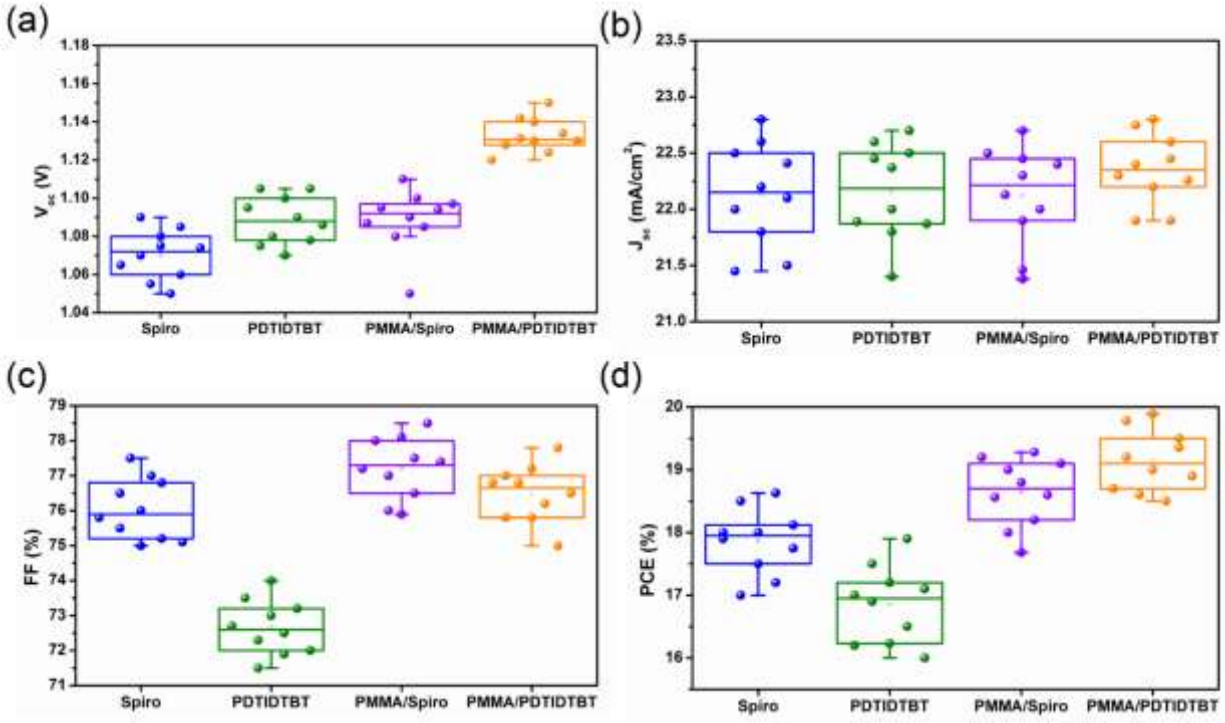

Figure S8. Statistics of the PV parameters for the PSCs with PDTIDTBT, spiro, PMMA/PDTIDTBT and PMMA/spiro HTLs.

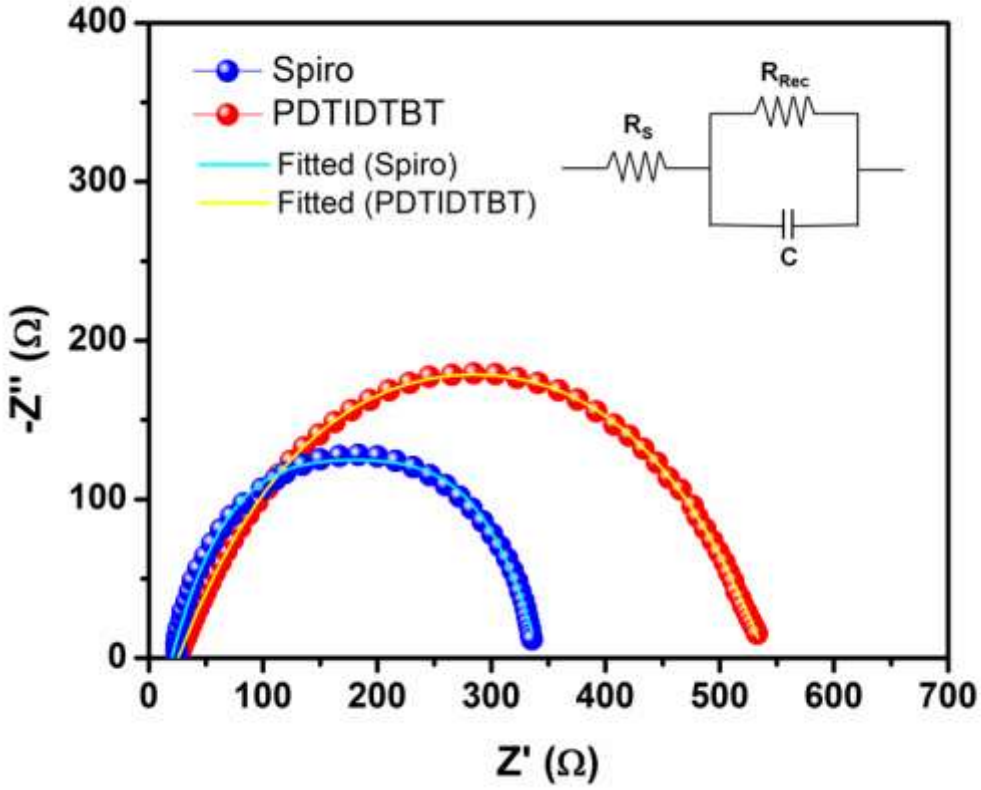

Figure S9. Nyquist plots of the PSCs with PDTIDTBT and spiro HTLs. The inset shows the fitting model.

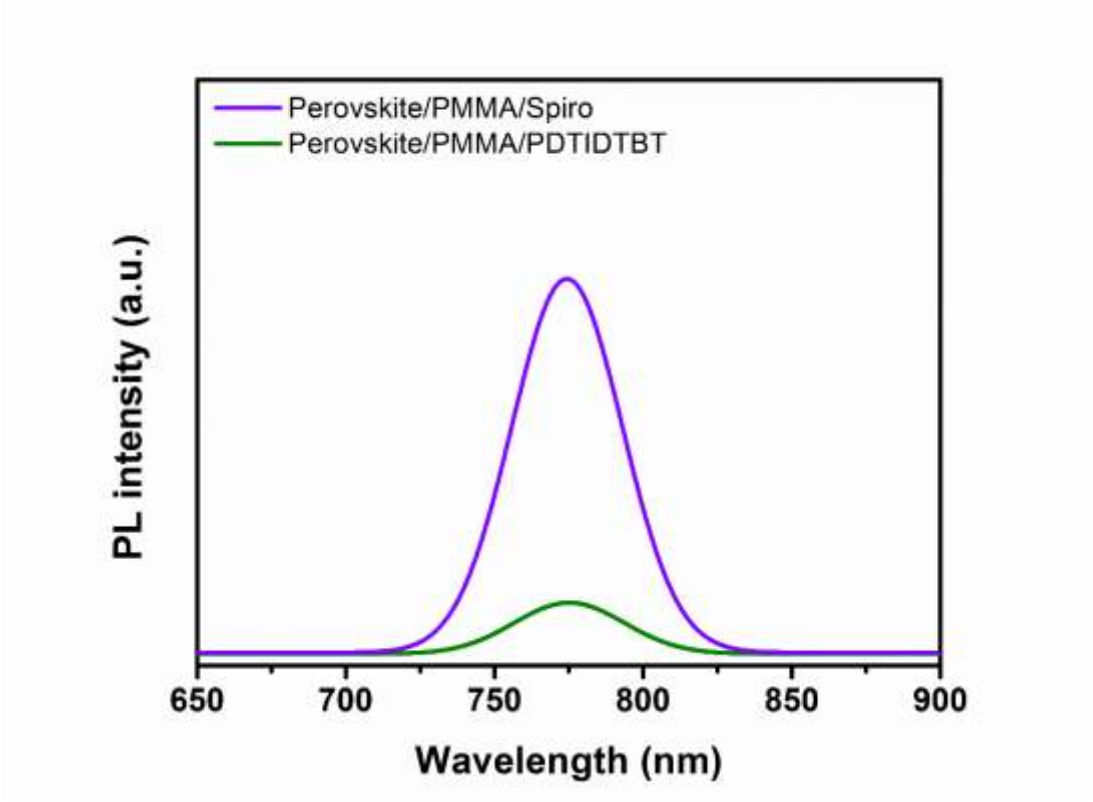

Figure S10. PL spectra of the perovskite/PMMA/PDTIDTBT and perovskite/PMMA/spiro samples coated on glass substrates.

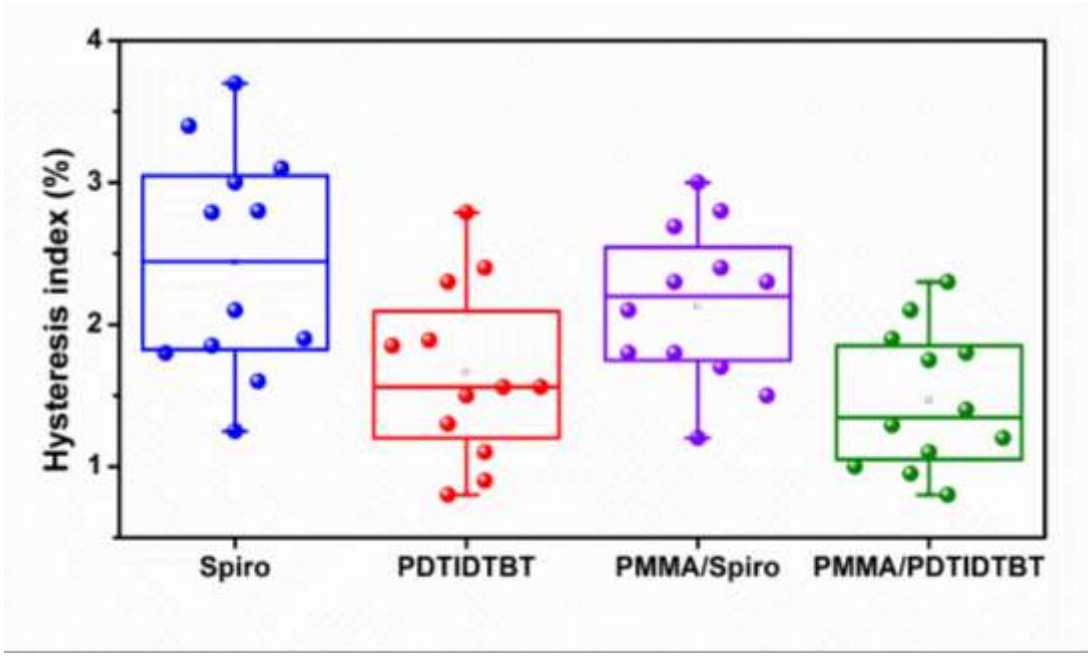

Figure S11. Statistics of the hysteresis indices (HIs) of the PSCs with PDTIDTBT, spiro, PMMA/PDTIDTBT and PMMA/spiro HTLs.

Table S1. Fitting parameters of the TRPL curves fitted by a biexponential equation for perovskite, perovskite/spiro, and perovskite/PDTIDTBT films.

Sample	**A_1**	**A_2**	**τ_1(ns)**	**τ_2(ns)**
Perovskite/glass	0.71	0.29	1.56	35.53
Perovskite/spiro	0.68	0.32	0.45	21.34
Perovskite/ PDTIDTBT	0.78	0.22	0.28	19.45

Here, we synthesize a new and dopant-free polymeric hole transporting layer, i.e., PDTIDTBT for mesoscopic perovskite solar cells and improve the efficiency and stability of the cells as compared to spiro-based devices.

TOC